J. Fluid Mech. (2011), *vol.* 681, *pp.* 154–172. © Cambridge University Press 2011
doi:10.1017/jfm.2011.219

Direct numerical simulation of spatially developing turbulent boundary layers with uniform blowing or suction

YUKINORI KAMETANI† AND KOJI FUKAGATA

Department of Mechanical Engineering, Keio University, Hiyoshi 3-14-1, Kohoku-ku, Yokohama 223-8522, Japan

(Received 2 August 2010; revised 3 March 2011; accepted 10 May 2011; first published online 23 June 2011)

Direct numerical simulation (DNS) of spatially developing turbulent boundary layer with uniform blowing (UB) or uniform suction (US) is performed aiming at skin friction drag reduction. The Reynolds number based on the free stream velocity and the 99 % boundary layer thickness at the inlet is set to be 3000. A constant wall-normal velocity is applied on the wall in the range, $-0.01U_\infty \leqslant V_{ctr} \leqslant 0.01U_\infty$. The DNS results show that UB reduces the skin friction drag, while US increases it. The turbulent fluctuations exhibit the opposite trend: UB enhances the turbulence, while US suppresses it. Dynamical decomposition of the local skin friction coefficient c_f using the identity equation (FIK identity) (Fukagata, Iwamoto & Kasagi, *Phys. Fluids,* vol. 14, 2002, pp. L73–L76) reveals that the mean convection term in UB case works as a strong drag reduction factor, while that in US case works as a strong drag augmentation factor: in both cases, the contribution of mean convection on the friction drag overwhelms the turbulent contribution. It is also found that the control efficiency of UB is much higher than that of the advanced active control methods proposed for channel flows.

Key words: boundary layer control, drag reduction, turbulent boundary layers

1. Introduction

The reduction of skin friction drag in turbulent flows is of great importance for mitigating their environmental impact, in particular for reducing fuel consumption in major transportation systems, such as aircrafts, trains and ships. Despite the extensive research conducted, a practical method for skin-friction drag reduction is still being explored.

A variety of ideas for skin-friction drag reduction have been examined, especially since the late 1980s following the emergence of direct numerical simulation (DNS) of wall-bounded turbulent flow (Kim, Moin & Moser 1987). These studies have recently been reviewed, e.g. by Kim (2003) on feedback control schemes, Kim & Bewley (2007) on linear control theory, Kasagi, Suzuki & Fukagata (2009) on hardware and practical control schemes and White & Mungal (2008) for friction drag reduction by polymer additives.

† Email address for correspondence: kametani@fukagata.mech.keio.ac.jp

https://doi.org/10.1017/jfm.2011.219 Published online by Cambridge University Press

Most of the previous numerical studies on friction drag reduction have dealt with internal flows, such as channel flows (see e.g. Kim 2003; Kim & Bewley 2007; Kasagi *et al.* 2009 and references therein). A theoretical framework is also better established for internal flows: for instance, we now know the mathematical relationship between the Reynolds stress and friction drag (Fukagata, Iwamoto & Kasagi 2002) and the theoretical limit of active friction drag reduction control for flows in a plane channel (Bewley 2009) and in arbitrary ducts (Fukagata, Sugiyama & Kasagi 2009). No such limit is currently known for external flows, however, as stated in the recent review by Choi, Jeon & Kim (2008).

In comparison to channel flows, far fewer studies have been reported for spatially developing boundary layers, even though practical friction drag reduction control should be targeted at external flows (since in internal flows, a slight increase in pipe diameter is sufficient to significantly reduce the pumping power). Park & Choi (1999), Kim, Sung & Chung (2002) and Kim, Kim & Sung (2003) performed DNS with steady blowing or suction from a spanwise localized slot. They concluded that blowing reduces the skin friction drag and suction increases it; blowing shifts the turbulence away from the wall and enhances it and suction has the opposite effect. Recently, Pamiès *et al.* (2007) performed large eddy simulations of a spatially developing turbulent boundary layer using the opposition control of Choi, Moin & Kim (1994). They also examined the case of uniform blowing (UB) in combination with opposition control. A larger drag reduction than that of opposition control alone was achieved.

Shear flows can be effectively modified by UB and uniform suction (US) from the wall, as exemplified by the film cooling used for turbine blades and slotted wings. The UB is also attractive as a means of reducing skin friction drag, as illustrated by the results of Pamiès *et al.* (2007) mentioned above. The modification of turbulence by UB and US has been studied in detail by Sumitani & Kasagi (1995) using direct numerical simulation (DNS) of turbulent channel flow. They found that the Reynolds stress increases on the blowing side and decreases on the suction side; by contrast, the friction drag reduces on the blowing side and increases on the suction side. This somewhat peculiar trend (also found in the blowing/suction slot case by Park & Choi 1999) was explained by an identity equation between the Reynolds stress and the friction drag (Fukagata *et al.* 2002). This identity equation (hereafter referred to as the FIK (Fukagata, Iwamoto & Kasagi) identity and described in detail in the next section) was applied to the Sumitani & Kasagi (1995) case and revealed the following mechanism: on the blowing side, where the Reynolds stress is increased, convection due to the mean wall-normal velocity contributes to drag reduction; the opposite was found on the suction side.

Since the upper boundary is open, one may have effects of UB or US somewhat different from those in channel flows, which is also expected from the difference between an uncontrolled channel flow and a spatially developing boundary layer (Monty *et al.* 2009). Clarifying how turbulence is modified by UB or US in external flow is also an important step towards their practical application.

In the present study, DNS of a spatially developing boundary layer is performed with UB or US. The mechanism of drag reduction or augmentation is investigated by using the FIK identity, and the control efficiency is discussed using efficiency indices (i.e. drag reduction rate, R, gain, G, and net energy saving rate, S), all defined in the next section.

https://doi.org/10.1017/jfm.2011.219 Published online by Cambridge University Press

2. Definitions of quantitative measures

2.1. *Decomposition of friction drag*

Fukagata *et al.* (2002) derived an exact mathematical relationship (FIK identity) between the Reynolds shear stress and the skin friction coefficient in fully developed channel and pipe flows, and in spatially developing boundary layers (for channel flow, Bewley & Aamo 2004 also derived a similar relationship). The FIK identity decomposes the friction coefficient into different dynamical contributions. The FIK identity (and some extended variants) has been used for quantifying the contribution of Reynolds stress to skin friction in incompressible flows (Fukagata *et al.* 2002) and compressible flows (Gomez, Flutet & Sagaut 2009) and quantitatively discussing the drag reduction mechanism by e.g. active control (Fukagata & Kasagi 2003), riblets (Peet & Sagaut 2009), addition of polymer or surfactant (Yu, Li & Kawaguchi, 2004; Hou, Somandepalli & Mungal 2008) and micro-bubbles (Xu *et al.* 2007; Sugiyama, Calzavarini & Lohse 2008). Furthermore, it has been used for designing new control schemes (Fukagata & Kasagi 2004; Min *et al.* 2006) and proposing a new scaling law and a new experimental friction determination technique for boundary layers (Hou, Somandepalli & Mungal 2006; Mehdi & White 2011).

For the spatially developing plane turbulent boundary layer, the local skin friction coefficient c_f is decomposed into four different dynamical contributions: the contributions from boundary layer thickness, c^δ, Reynolds shear stress, c^T, mean convection, c^C, and spatial development, c^D, i.e.

$$c_f(x) = \underbrace{\frac{4(1-\delta_d)}{Re_\delta}}_{c^\delta(x)} \underbrace{+2\int_0^1 2(1-y)(-\overline{u'v'})\mathrm{d}y}_{c^T(x)} \underbrace{+2\int_0^1 2(1-y)\,(-UV)\,\mathrm{d}y}_{c^C(x)} \underbrace{-2\int_0^1 (1-y)^2\left(\frac{\partial UU}{\partial x}+\frac{\partial \overline{u'u'}}{\partial x}-\frac{1}{Re}\frac{\partial^2 U}{\partial x \partial x}\right)\mathrm{d}y}_{c^D(x)}, \quad (2.1)$$

where δ_d is the dimensionless displacement thickness and all the variables are non-dimensionalized by the free stream velocity U_∞ and the local 99 % boundary layer thickness δ. Note that the mean convection term c^C and the spatial development term c^D are absent in fully developed channel and pipe flows.

2.2. *Control efficiency*

In practical applications, it is not enough to consider only the level of friction drag reduction. One must also consider the efficiency of control. Considering only an ideal control input (viz. neglecting any mechanical energy loss in actuators/sensors), the drag reduction rate, R, gain, G, and net energy saving rate, S, can be defined as (see e.g. Kasagi, Hasegawa & Fukagata 2009)

$$R = \frac{W_0 - W}{W_0}, \quad (2.2)$$

$$G = \frac{W_0 - W}{W_{in}} \quad (2.3)$$

and

$$S = \frac{W_0 - (W + W_{in})}{W_0}, \quad (2.4)$$

https://doi.org/10.1017/jfm.2011.219 Published online by Cambridge University Press

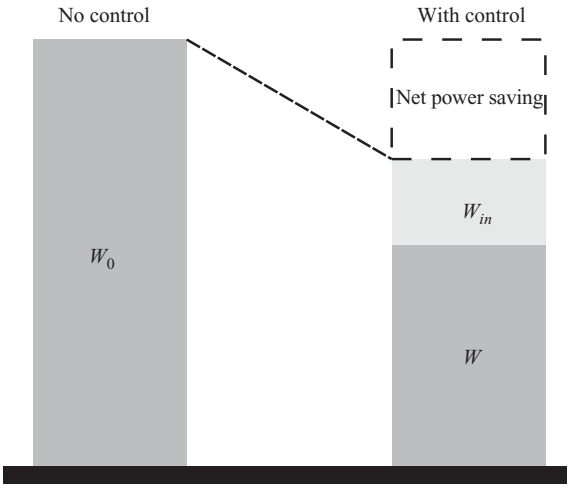


FIGURE 1. Schematic of control efficiency.

where W_0 and W are the pumping powers in the uncontrolled and controlled cases, respectively, and W_{in} denotes the power of the (ideal) control input. A schematic of the relationship between R and S is illustrated in figure 1.

3. Numerical procedure

The governing equations are the incompressible continuity and Navier–Stokes equations, i.e.

$$\frac{\partial u_i}{\partial x_i} = 0, \tag{3.1}$$

$$\frac{\partial u_i}{\partial t} = -\frac{\partial u_i u_j}{\partial x_j} - \frac{\partial p}{\partial x_i} + \frac{1}{Re}\frac{\partial^2 u_i}{\partial x_j \partial x_j}, \tag{3.2}$$

where x_i $(i = 1, 2, 3)$ are the Cartesian coordinates and u_i are the corresponding velocity components. All variables are non-dimensionalized by the free stream velocity U_∞ and the 99 % boundary layer thickness at the inlet of the computational domain δ_0. The Reynolds number is defined as $Re = U_\infty \delta_0 / \nu$, where ν is the kinematic viscosity.

The DNS code is based on a channel flow code developed by Fukagata, Kasagi & Koumoutsakos (2006), which was itself adapted from a pipe flow code (Fukagata & Kasagi 2002). The spatial discretization uses the energy-conservative second-order finite difference scheme (e.g. Ham, Lien & Strong 2002). The time integration uses the low-storage third-order Runge–Kutta/Crank–Nicolson scheme (e.g. Spalart, Moser & Rogers 1991).

The computational domain is composed of two regions: a driver region and a main region, as shown in figure 2. The recycle method of Lund, Wu & Squires (1998) is used in the driver region to generate the inflow condition.

In both the driver and main regions, the upper boundary conditions for the streamwise velocity, u, the wall-normal velocity, v, and the spanwise velocity, w, are set to be $\partial u/\partial y = \partial v/\partial y = 0$ and $w = 0$. On the wall, the no-slip condition is applied in the driver region, while in the main region UB or suction velocity $v = V_{ctr}$ is added.

https://doi.org/10.1017/jfm.2011.219 Published online by Cambridge University Press

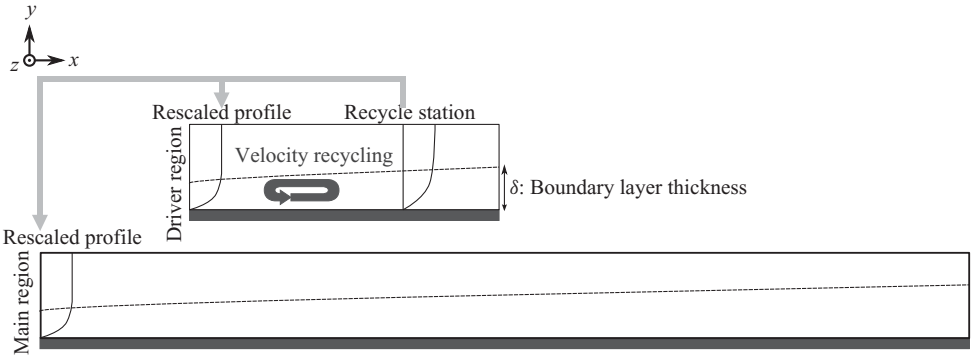


FIGURE 2. Computational geometry.

The convective boundary condition is applied at the downstream end of each computational domain, i.e.

$$\frac{\partial u_i}{\partial t} + \overline{u}(y)\frac{\partial u_i}{\partial x} = 0, \tag{3.3}$$

where $\overline{\cdot}$ denotes the average in the homogeneous (i.e. spanwise) direction. The pressures at the inlet and outlet boundaries are given by the Navier–Stokes characteristic boundary condition of Miyauchi, Tanahashi & Suzuki (1996),

$$\frac{\partial p}{\partial t} + U_\infty \frac{\partial p}{\partial x} = \frac{1}{2Re}\omega_z^2, \tag{3.4}$$

where ω_z denotes the spanwise vorticity. It is known that this boundary condition considerably suppresses the unphysical pressure near the inlet and outlet that appears when an ordinary Neumann condition is used.

The streamwise, wall-normal and spanwise lengths of the driver and main regions are $(L_x^D, L_y^D, L_z^D) = (3\pi\delta_0, 3\delta_0, \pi\delta_0)$ and $(L_x, L_y, L_z) = (9\pi\delta_0, 3\delta_0, \pi\delta_0)$, respectively, where the superscript D denotes the driver region. The corresponding numbers of grid points are $(N_x^D, N_y^D, N_z^D) = (128, 96, 128)$ and $(N_x, N_y, N_z) = (512, 96, 128)$, respectively. The recycle station is located at $x^D = 2\pi\delta_0$. In this study, the Reynolds number $Re = U_\infty\delta_0/\nu$ is set to be 3000, which corresponds to an inlet friction Reynolds number of $Re_{\tau 0} = u_\tau\delta_0/\nu \simeq 160$, where u_τ is the friction velocity. The grid spacings in the streamwise and spanwise directions (in wall units) are $\Delta x^{+0} = 8.83$ and $\Delta z^{+0} = 3.93$, respectively, where the superscript $^{+0}$ denotes the wall unit based on the friction velocity at the inlet of the main part. The minimum grid spacing in the wall-normal direction is $\Delta y^{+0} = 0.47$ and the maximum spacing is $\Delta y^{+0} = 6.67$.

The statistics are gathered over a time period of $T^{+0} \approx 4000$. The start of this time period is well after a statistical steady state has been reached.

4. Results and discussion

4.1. *Base flow*

The spatial development of the boundary layer is presented in figure 3. Figure 3(*a*) shows the spatial development of the momentum thickness Reynolds number $Re_\theta = U_\infty\theta/\nu$; the displacement thickness $Re_d = U_\infty\delta_d/\nu$, and the shape factor H in the uncontrolled turbulent boundary layer. The momentum thickness and the displacement thickness are both developing in the downstream direction. Moreover, a negative gradient of the shape factor indicates that the momentum towards the

https://doi.org/10.1017/jfm.2011.219 Published online by Cambridge University Press

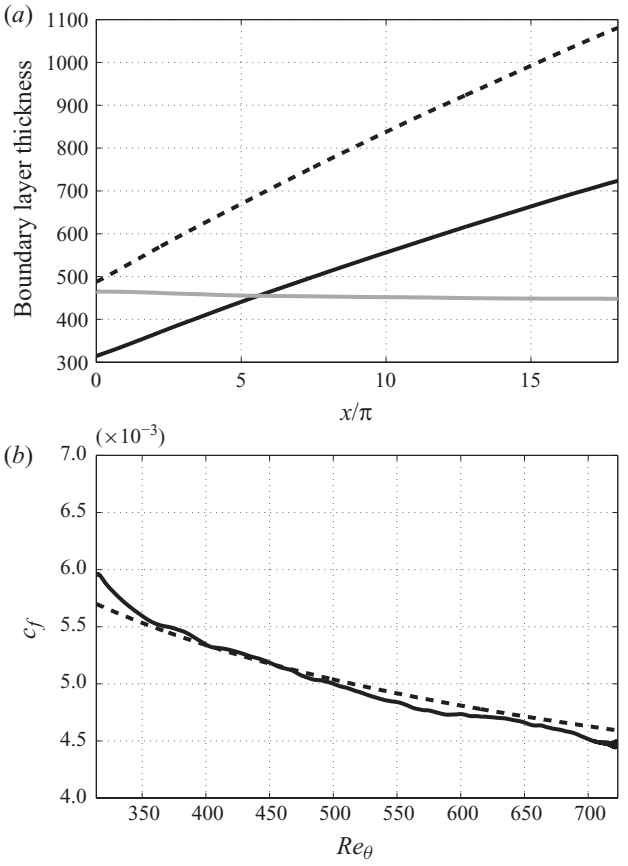


FIGURE 3. Spatial development of the boundary layer. (a) Boundary layer thickness and shape factor as a function of x: solid black line, Re_θ; dashed black line, Re_{δ_d}; solid grey line, shape factor $300H$. (b) Local friction coefficient c_f: solid line, c_f computed from wall shear stress; dashed line, c_f of empirical formula.

wall due to the turbulent transport increases as the Reynolds number increases. The boundary layer thickness develops from δ_0 at the inlet to about $2.0\,\delta_0$ at the downstream end. The development of the local skin friction coefficient, $c_f = 2\tau_w/\rho U_\infty^2$, is presented in figure 3(b) as a function of Re_θ. A slight deviation from the power law-based formula (Schoenherr 1932)

$$c_f \approx 0.31[\ln^2(2Re_\theta) + 2\ln(2Re_\theta)]^{-1} \tag{4.1}$$

is found, and this is likely due to the low Reynolds number. A similar deviation has also been reported in Kong, Choi & Lee (2000).

The velocity statistics at several streamwise locations are presented in figure 4. Figure 4(a) shows the mean velocity profile at $Re_\theta = 530$ and 700. In the regions near the wall, the profile is in reasonable agreement with the DNS result of Wu & Moin (2009) at $Re_\theta = 700$. Figure 4(b) shows the root-mean-square (r.m.s.) velocity fluctuation. The strongest fluctuation appears in the streamwise component u_{rms}. The peak of u_{rms} is found at $y^+ \approx 15$ regardless of the Reynolds number within the present Reynolds number range. The peaks of v_{rms} and w_{rms} are found to shift away from the wall as the Reynolds number increases. The viscous shear stress (VSS) $\partial U/\partial y$ and the

https://doi.org/10.1017/jfm.2011.219 Published online by Cambridge University Press

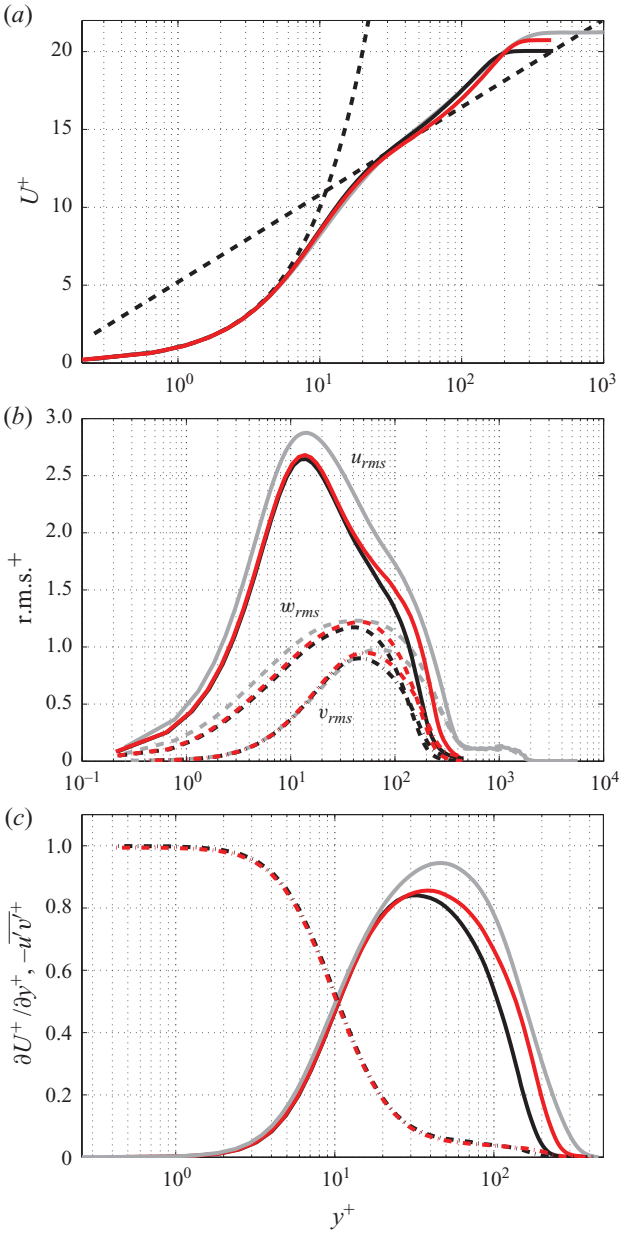


FIGURE 4. Base flow statistics: black lines, $Re_\theta = 530$; red lines, $Re_\theta = 700$; grey lines, Wu & Moin (2009) at $Re_\theta = 700$. (*a*) Mean streamwise velocity, U (dashed lines represent the law of the wall). (*b*) Turbulent intensities: solid, u_{rms}; dashed, v_{rms}; chain, w_{rms}. (c) Shear stresses: solid, Reynolds shear stress; dashed viscous shear stress.

Reynolds shear stress (RSS) $-\overline{u'v'}$ are shown in figure 4(*c*). As the Reynolds number increases, the peak value of RSS becomes larger and the location of the peak shifts away from the wall, while there is almost no difference in the VSS profiles.

Some difference can be found between the present results and those of Wu & Moin (2009). Namely, U, u_{rms} and $-\overline{u'v'}$ are slightly larger in the present simulation. These differences may be attributed to the difference in the upstream conditions. The

https://doi.org/10.1017/jfm.2011.219 Published online by Cambridge University Press

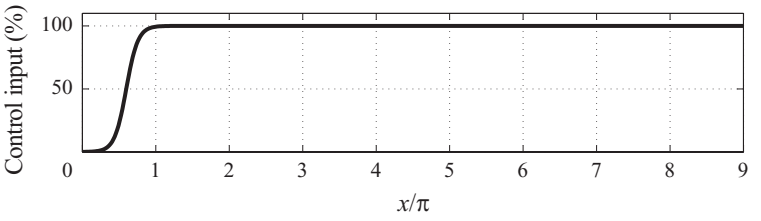


FIGURE 5. Control input profile.

recycle method is used in the present simulation, which assumes a fully developed turbulence. In Wu & Moin (2009), in contrast, a transition from the laminar boundary layer is reproduced, due to which the flow at this Re_θ appears still transitional (see Appendix). In addition, the difference may also be attributed to the difference in the grid resolution: $\Delta x^{+0} = 8.83$ and $\Delta z^{+0} = 3.93$ in the present simulation, but $\Delta x^{+0} = 5.91$ and $\Delta z^{+0} = 11.13$ in Wu & Moin (2009). It is known that low resolution in the spanwise direction causes an underestimation of redistribution from u' to v' and w' components (Kajishima 2003) (see Appendix).

4.2. *Uniform blowing or suction*

In the present study, the magnitude of UB or US is set to be 0.1 %, 0.5 % or 1.0 % of free stream velocity. A transition zone is placed at $0 \leqslant x \leqslant \pi$, in which the control amplitude is gradually increased by using a hyperbolic tangent function as shown in figure 5 (see Appendix for more detail).

The effect of UB/US on the spatial development is presented in figure 6. It is found from the development of momentum thickness in figure 6(a) that UB thickens the boundary layer, while US thins it. The magnitude of both effects depends on the amplitude of UB/US. The shape factor H shown in figure 6(b) indicates that UB increases H and US decreases it. The UB (US) works to push (pull) the mean velocity profile away from (towards) the wall, leading to the effects observed above as if the Reynolds number is increased by UB and decreased by US. An interesting observation in the UB case is that the shape factor increases in the downstream region, since the shape factor usually decreases as the Reynolds number increases.

The local friction coefficient c_f shown in figure 6(c) clearly indicates that UB reduces the friction drag, while US enhances it. This is basically due to the modification of the mean velocity profile as shown in figure 7(a); it is shifted away from the wall by UB, but shifted towards the wall by US. Note that the quantities shown in figure 7 are non-dimensionalized by the local friction velocity of the uncontrolled flow at the same streamwise position (denoted by the superscript $+nc$). Profiles of the viscous and Reynolds shear stresses shown in figure 7(b) indicate that UB (US) reduces (enhances) the VSS, but enhances (reduces) the Reynolds shear stress. This opposite effect, which is counterintuitive, is similar to that observed in a channel flow with UB on one wall and US on the other wall (Sumitani & Kasagi 1995).

Here, the global skin friction drag coefficients, C_f, is defined as

$$C_f = \frac{1}{L_{ctr}} \int_0^{L_{ctr}} c_f \, \mathrm{d}x. \tag{4.2}$$

The drag reduction rate, R, as introduced in § 2.2 is expressed by using the global friction coefficients as

$$R = \frac{C_{f,nc} - C_{f,ctr}}{C_{f,nc}}, \tag{4.3}$$

https://doi.org/10.1017/jfm.2011.219 Published online by Cambridge University Press

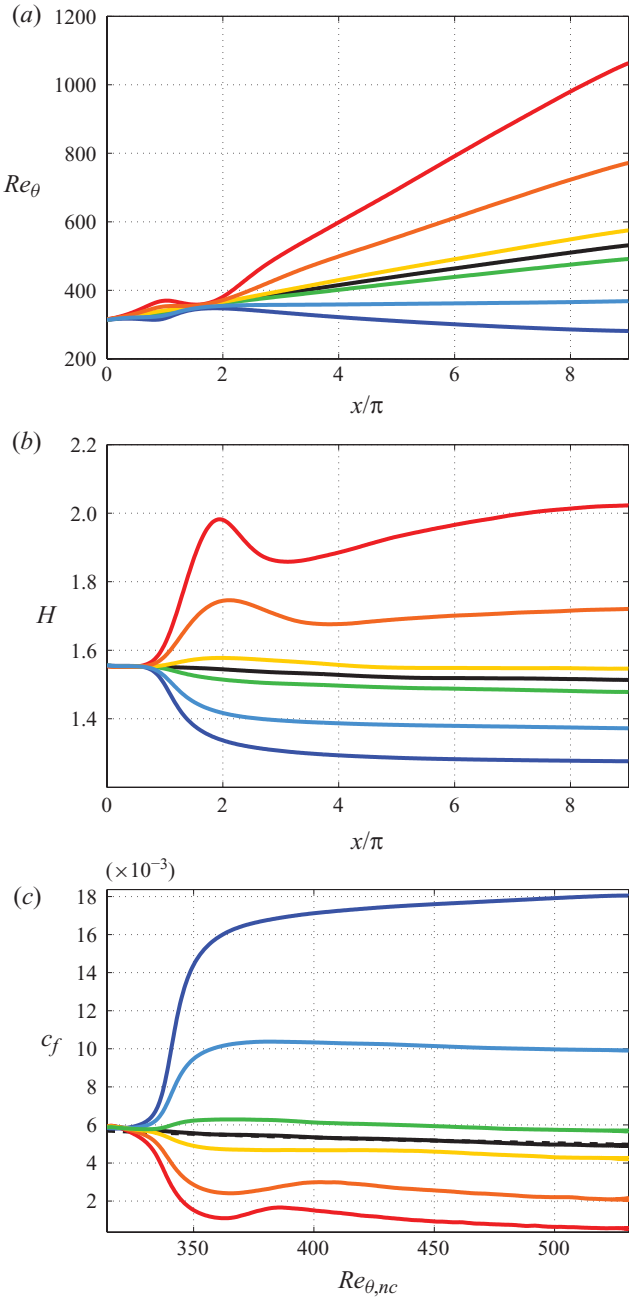


FIGURE 6. Effect of UB/US on spatial development of the boundary layer: black, no control; yellow, 0.1 % UB; orange, 0.5 % UB; red, 1 % UB; green, 0.1 % US; light blue, 0.5 % US; blue, 1 % US. (*a*) Momentum thickness Re_θ. (*b*) Shape factor H. (*c*) Local friction coefficient.

where $C_{f,nc}$, $C_{f,ctr}$ and L_{ctr} denote the friction coefficients of the flow with and without blowing/suction and the streamwise length of the computational domain, respectively. Figure 8 shows the drag reduction rate, R, as a function of wall-normal velocity applied on the wall, V_{ctr}. It is found that increasing the amplitude of UB or US results in larger drag reduction or drag augmentation, respectively. In addition,

https://doi.org/10.1017/jfm.2011.219 Published online by Cambridge University Press

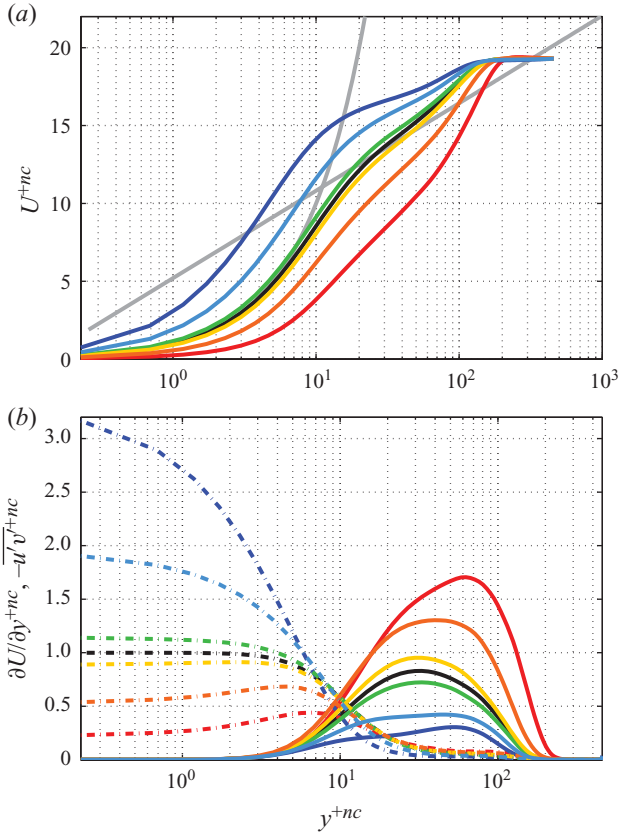


FIGURE 7. Effect of UB/US on statistics as a function of y^{+nc} at the location of $Re_{\theta,nc} = 430$: black, no control; yellow, 0.1 % UB; orange, 0.5 % UB; red, 1 % UB; green, 0.1 % US; light blue, 0.5 % US; blue, 1 % US. (*a*) Streamwise mean velocity. (*b*) Shear stresses: solid, Reynolds shear stress; dashed, VSS.

the relationship between the drag reduction rate, R, and the control amplitude is found to be nonlinear.

The instantaneous flow structures are shown in figure 9 by the second invariant of the deformation tensor Q^{+0} and the wall shear stress τ_w^{+0}. Compared to the uncontrolled case, vortices are enhanced in the UB case in spite of the reduced wall shear stress, while in the US case vortices are suppressed despite the increase of wall shear stress.

4.3. *Analysis using the FIK identity*

In order to quantitatively investigate different dynamical effects of UB/US on the friction drag, the local friction coefficient c_f is decomposed into four different dynamical components as defined in (2.1). Each component computed from the statistics is shown in figure 10. In the upstream region, some discrepancy is found between c_f directly computed from the wall shear (dashed line) and that using (2.1) (black solid line), especially in the UB and US cases. This may be due to the non-zero mean pressure gradient caused by the sudden application of blowing/suction, while the mean pressure gradient is assumed to be zero in the derivation of (2.1): in fact such non-zero pressure gradient is observed in the statistics. In the following, a discussion

https://doi.org/10.1017/jfm.2011.219 Published online by Cambridge University Press

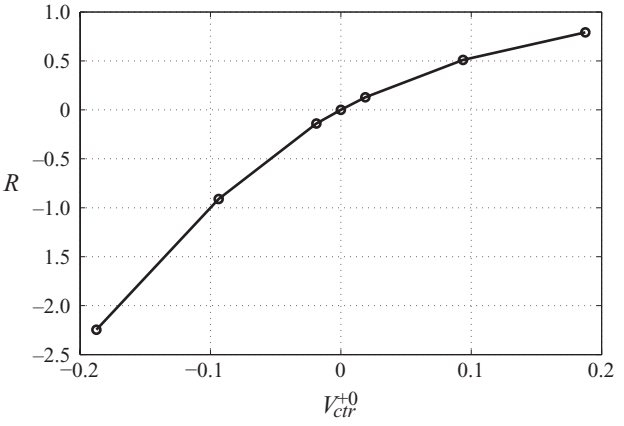


FIGURE 8. Drag reduction rate as a function of control amplitude.

is made of the downstream (i.e. fully developed) region where this discrepancy is reasonably small.

In spatially developing boundary layers, some terms in the FIK identity act to increase friction drag, while others act to reduce it. In the base flow (figure 10*a*), the contributions from the Reynolds stress (c^T) and the streamwise development (c^D) work to increase friction drag (i.e. $c^T > 0$, $c^D > 0$), while the contribution from the mean convection (c^C) works to reduce it (i.e. $c^C < 0$). In the UB case (figure 10*b*), all the components except for c^δ are increased while keeping their signs. In the US case, in contrast, the mean convection term c^C changes to a strong drag augmentation factor and the spatial development term c^D works as a weak reduction factor. From these analyses, we can conclude that the mean convection term c^C which includes $-UV$ has a very important role in determining whether drag reduction or augmentation occurs by UB/US. This argument is more clearly illustrated by the decomposition of the global friction coefficient C_f, i.e.

$$\begin{aligned} C_f &= \frac{1}{L_{ctr}} \int_0^{L_{ctr}} c_f \, \mathrm{d}x \\ &= \frac{1}{L_{ctr}} \int_0^{L_{ctr}} c^\delta \, \mathrm{d}x + \frac{1}{L_{ctr}} \int_0^{L_{ctr}} c^T \, \mathrm{d}x + \frac{1}{L_{ctr}} \int_0^{L_{ctr}} c^C \, \mathrm{d}x + \frac{1}{L_{ctr}} \int_0^{L_{ctr}} c^D \, \mathrm{d}x \\ &= C^\delta + C^T + C^C + C^D. \end{aligned} \tag{4.4}$$

Figure 11 clearly illustrates that in the UB case the negative contribution from the mean convection term C^C is greater than the positive contribution of Reynolds stress C^T, while in the US case the positive contribution from C^C is larger than the decrease in C^T.

4.4. *Control efficiency*

The control efficiency is briefly discussed here in terms of the drag reduction rate, R, gain, G, and net energy saving rate, S, as introduced in § 2.2. These measures can be expanded by using the global skin friction coefficients, as

$$G = \frac{C_{f,nc} - C_{f,ctr}}{W_{in}/L_{ctr}}, \tag{4.5}$$

https://doi.org/10.1017/jfm.2011.219 Published online by Cambridge University Press

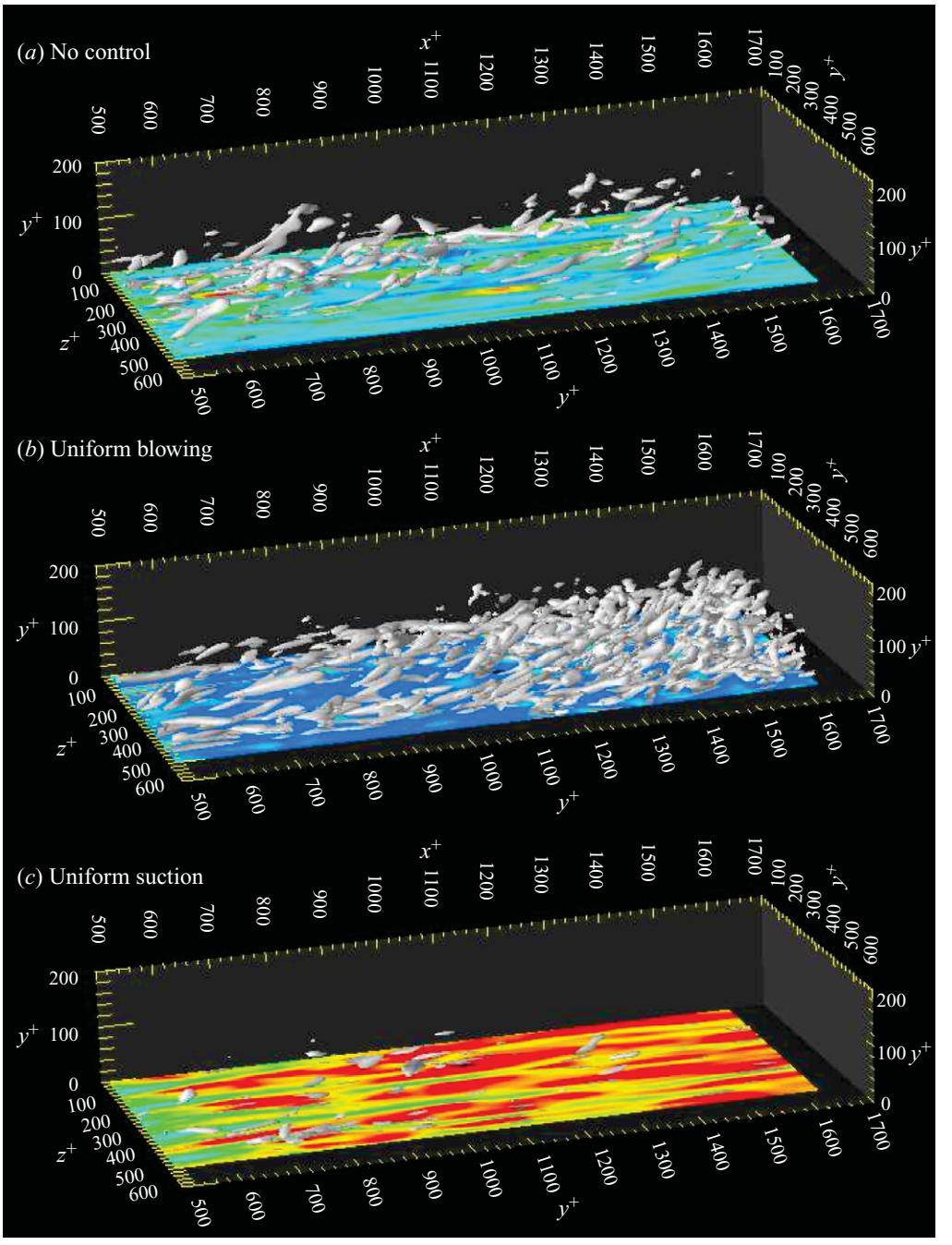


FIGURE 9. Visualization of flow in the control region using the second invariant of the deformation tensor Q^{+0} and contours of the wall shear stress τ_w^{+0}: (*a*) no control, (*b*) 1 % UB and (*c*) 1 % US.

$$S = \frac{C_{f,nc} - (C_{f,ctr} + W_{in}/L_{ctr})}{C_{f,nc}}, \tag{4.6}$$

where $C_{f,nc}$ and $C_{f,ctr}$ denote the friction coefficients of the flow with and without blowing/suction, respectively, and L_{ctr} is the streamwise length of the computational

https://doi.org/10.1017/jfm.2011.219 Published online by Cambridge University Press

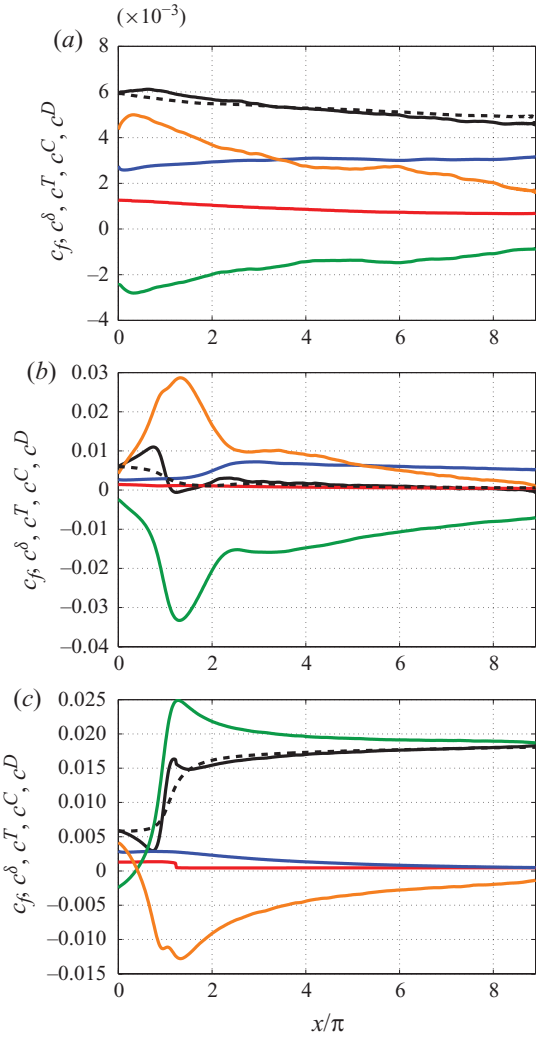


FIGURE 10. Each term of the FIK identity affected by UB/US control: (*a*) no control, (*b*) 1 % UB and (*c*) 1 % US. Black, FIK total; red, c^{δ}; blue, c^{T}; green, c^{C}; orange, c^{D}; dashed line, c_f from $\partial U/\partial y$ on the wall.

domain. Note that the driving powers for the flows with control W and without control W_0 are equivalent to $C_{f,ctr}L_{ctr}$ and $C_{f,nc}L_{ctr}$, respectively. The input power W_{in} for UB/US is computed as

$$W_{in} = \int_0^{L_{ctr}} \left[(P_w - P_{w-})\, V_{ctr} + \frac{1}{2} V_{ctr}^3 \right] \mathrm{d}x, \tag{4.7}$$

where P_{w-} denotes the mean pressure on the opposite side of the wall where the blowing device is connected. Hereafter, the first term on the right-hand side is neglected by assuming no pressure difference between P_w and P_{w-}. This is the most optimistic definition.

In figure 12, G and S computed from the wall shear are shown as an $S-G$ map. The values reported in the previous studies on internal flows are also presented for

https://doi.org/10.1017/jfm.2011.219 Published online by Cambridge University Press

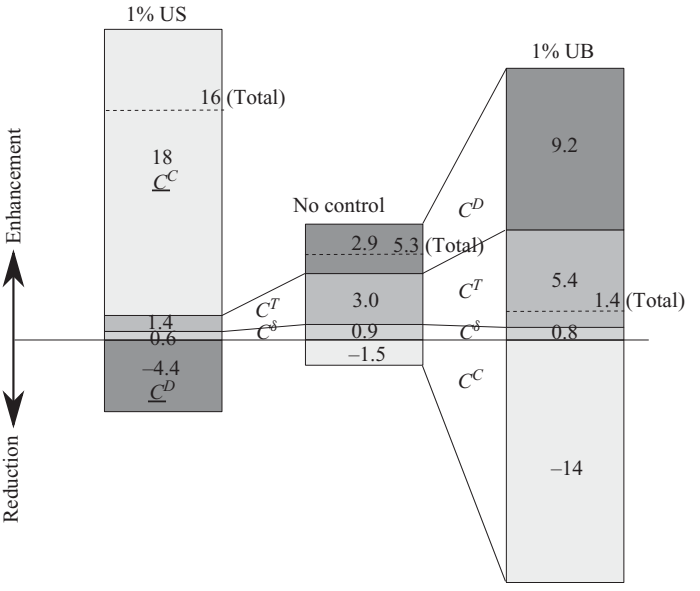


FIGURE 11. Different dynamical contributions to the global friction drag coefficient ($\times 10^3$).

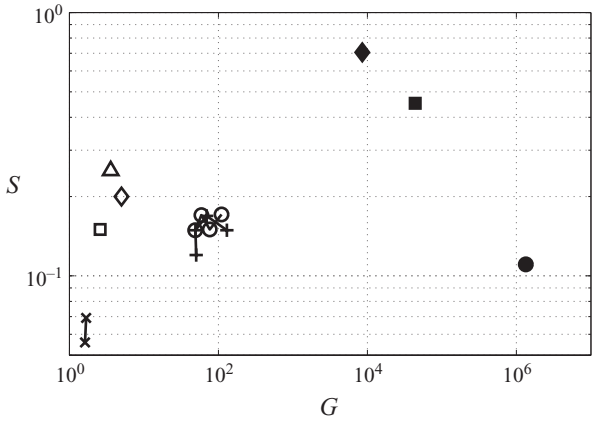


FIGURE 12. Net energy saving rate achieved by different active control schemes: ○, Choi *et al.* (1994)'s opposition control (computed by Iwamoto *et al.* 2002 at a different Reynolds number); +, Lee *et al.* (1998)'s suboptimal control (Iwamoto *et al.* 2002); ×, temporally periodic spanwise wall-oscillation (Quadrio & Ricco 2004); ◇, streamwise travelling wave (Min *et al.* 2006); □, steady streamwise forcing (Xu *et al.* 2007); △, spatially periodic spanwise oscillation (Yakeno *et al.* 2009). Solid markers denote UB in the present simulation: ◆, 1 % UB; ■, 0.5 % UB; ●, 0.1 % UB.

comparison. As compared to the values in the active control of internal flow, UB gives much higher efficiency.

From more practical viewpoint, the pressure difference between P_w and P_{w-} should be considered. For example, if we apply this blowing for a high-speed train with an intake placed on the front, the pressure loss in the duct leading to the blowing device may become extremely large (in fact, how to supply the air itself is a formidable engineering issue). Therefore, the actual control efficiency should be much less than the ideal value presented here.

https://doi.org/10.1017/jfm.2011.219 Published online by Cambridge University Press

4.5. *Reynolds number effect*

While the present study deals with low Reynolds number turbulence, control effect at high Reynolds number should be a crucial concern towards practical applications. The present analysis enables us to make a rough estimation of the Reynolds number effect. As clearly observed above, the Reynolds stress term (c^T) contributes to increase the drag and the mean convection term (c^C) reduces the drag in the blowing case; the stronger effect of the latter eventually leads to the drag reduction. Since these two terms are considered dominant also at high Reynolds number, the ratio of $-UV$ to $-\overline{u'v'}$ (i.e. integrands of c^C and c^T) should be a good indicator whether the drag reduction effect becomes stronger or weaker. The log-law of wall turbulent flow with UB/suction is expressed as (Stevenson 1963)

$$\frac{2}{V_{ctr}^+}\left(\sqrt{1+V_{ctr}^+U^+}-1\right)\approx\frac{1}{\kappa}\ln(y^+)+B, \tag{4.8}$$

where κ and B are constants. By using this, the ratio of $-UV$ to $-\overline{u'v'}$ can be estimated as

$$\frac{-UV|_{ctr}}{-\overline{u'v'}}=\frac{-U^+V^+|_{ctr}}{-\overline{u'v'}^+}\sim\frac{U_\infty^+V_{ctr}^+}{1}=\frac{V_{ctr}}{U_\infty}U_\infty^{+2}\sim\frac{V_{ctr}}{U_\infty}\ln^2(Re_\tau). \tag{4.9}$$

This estimate suggests that if the blowing amplitude is constant with respect to the free stream velocity, i.e. $V_{ctr}/U_\infty=$ const., the drag reduction effect is stronger at higher Reynolds number.

5. Concluding remarks

The DNSs of a spatially developing boundary layer with UB or US were performed. It was found that UB reduces friction drag and enhances turbulence, while US enhances friction drag and suppress turbulence, similar to blowing/suction slot and UB and US applied in channel flow, previously studied. Quantitative analysis using the FIK identity revealed that the mean convection term works as a drag reduction factor in the uncontrolled spatially developing boundary layer, while the Reynolds shear stress term and the spatial development term work as drag augmentation factors. The mean convection term has a very important role in determining whether drag reduction or drag augmentation occurs by UB/US: the drag reduction in the UB case is attributed to the negative contribution from the mean convection term; likewise, the drag augmentation in the US case is due to the positive contribution from the mean convection term. In fully developing internal flows, the suppression of turbulence is a major strategy in reducing drag, as is mathematically implied by the FIK identity. In spatially developing boundary layers, in contrast, use of the mean convection term is considered the efficient way of reducing the friction drag, even if it increases turbulence away from the wall.

An order-of-magnitude analysis suggests that the drag reduction effect may be stronger at higher Reynolds number if the blowing amplitude relative to the free stream velocity is fixed. Details of high Reynolds number flows including the effect of very large-scale motion (see e.g. Marusic, Mathis & Hutchins 2010), however, should be investigated further. There also remains another practical issue: how to get mass for UB. This issue is highly dependent on the geometrical shape of control target. For an aerofoil, for instance, it may be possible to apply suction near the leading edge to suppress the transition and to apply blowing near the trailing edge to reduce the

https://doi.org/10.1017/jfm.2011.219 Published online by Cambridge University Press

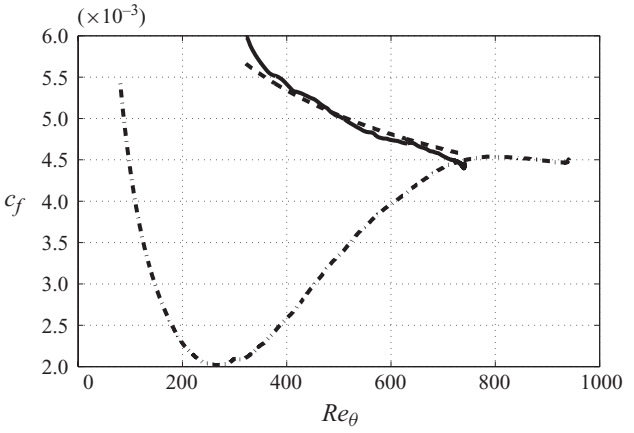


FIGURE 13. Friction coefficient in whole computational domain: solid line, simulation in this paper; dashed line, empirical formula from momentum thickness in this paper; chain line, Wu & Moin (2009).

friction of developed turbulence; but it might be more difficult for objects like bullet trains. These practical issues remain open for future work.

The authors are grateful to Drs Shinnosuke Obi and Simon Illingworth (Keio University), Drs Nobuhide Kasagi and Yosuke Hasegawa (The University of Tokyo), Dr Kaoru Iwamoto (Tokyo University of Agriculture and Technology) and Dr Yoshitsugu Naka (Ecole Centrale Lille) for fruitful discussion. We also thank Dr Parviz Moin (Stanford University) and Dr Xiaohua Wu (Royal Military College of Canada) for comments concerning the baseline results. This work was supported through Grant-in-Aid for Scientific Research (A) (No. 20246036) by the Ministry of Education, Culture, Sports and Technology of Japan (MEXT), the silent supersonic aircraft research program of the Japan Aerospace Exploration Agency (JAXA), and the Keio University Global COE program, the Center for Education and Research of Safe, Secure and Symbiotic System Design.

Appendix. Numerical concerns

There are two major differences between the present simulations and those of Wu & Moin (2009), which might have caused the difference in the statistics at $Re_\theta = 700$: the upstream condition and the resolution in the spanwise direction. As for the upstream condition, Wu & Moin (2009) reproduce the transition in the upstream region, while the present study adopts the recycle method assuming fully developed turbulence. The friction coefficient shown in figure 13 suggests that Wu & Moin (2009)'s flow is under a transitional regime in the Re_θ range considered in our simulation (i.e. up to $Re_\theta = 700$). The dependency on the spanwise resolution has also been examined. The turbulent intensity at $\Delta z^{+0} = 4$ (fine grid used in the present simulation) and 16 (coarse grid) shown in figure 14 clearly indicates that u_{rms} increases and v_{rms} and w_{rms} decrease as the spanwise grid becomes coarser. Considering the two differences above, it can be easily understood that our results with $\Delta z^{+0} = 16$ agree better with those of Wu & Moin (2009) at $Re_\theta = 800$ (at which the flow is considered to be fully developed). There are still some difference in the region away from the wall, which might be due to the artificial techniques used in both methods and the difference in the wall-normal extent of the computational domain.

https://doi.org/10.1017/jfm.2011.219 Published online by Cambridge University Press

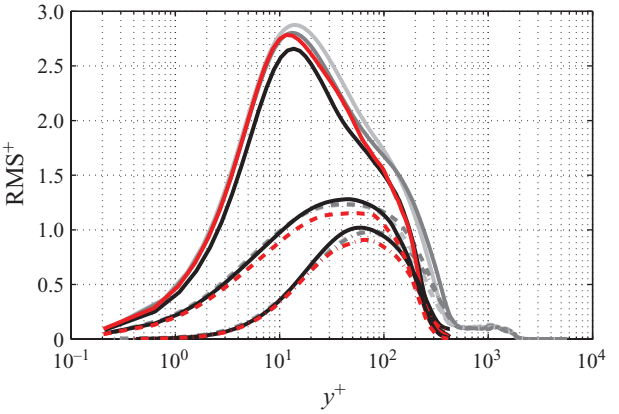


FIGURE 14. Turbulent intensities: black, $Re_\theta = 700$ (present); red, $Re_\theta = 700$ (coarse); light grey, $Re_\theta = 700$ (Wu & Moin 2009); dark grey, $Re_\theta = 800$ (Wu & Moin 2009). Solid, u_{rms}; dashed, v_{rms}; chain, w_{rms}.

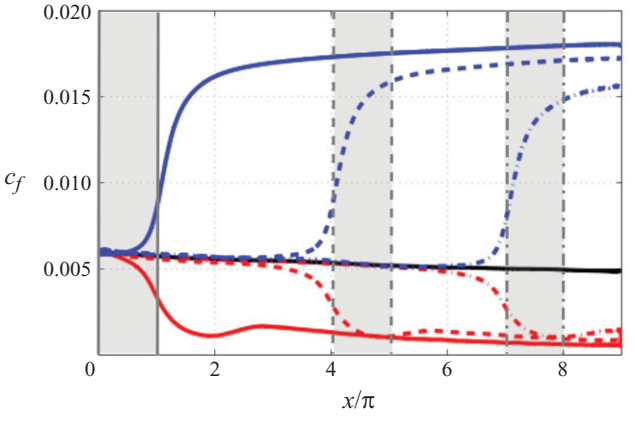


FIGURE 15. Effect of positions of control starting zone: black, no control; red, UB; blue, US. Solid, $0 \leqslant x_s/\delta_0 \leqslant \pi$; dashed, $4\pi \leqslant x_s/\delta_0 \leqslant 5\pi$; chain, $7\pi \leqslant x_s/\delta_0 \leqslant 8\pi$. Grey mask, control starting zone.

In the present simulation, UB or US is switched on in the control part. Although the magnitude of blowing/suction is gradually changed as shown in figure 5, it may affect the upstream flow, too. Therefore, dependency on the position where the blowing/suction starts, x_s has been examined by using 1 % UB/US. Figure 15 shows the streamwise development of local skin friction coefficient, c_f, for different x_s. The change of boundary condition is observed to affect c_f in the region up to π upstream. In the case of $x_s = 4\pi$, for instance, c_f is found to deviate from the uncontrolled value in the region of $x > 3\pi$, but the profile in the further upstream region collapses with the uncontrolled profile. In the downstream region, the development of c_f is found to be similar unless the blowing region is too short. Judging from these results, we set $x_s = 0$ in the main simulations, since it is desirable to take the statistically steady region as large as possible.

https://doi.org/10.1017/jfm.2011.219 Published online by Cambridge University Press

REFERENCES

Bewley, T. R. 2009 A fundamental limit on the balance of power in a transpiration-controlled channel flow. *J. Fluid Mech.* **632**, 443–446.

Bewley, T. R. & Aamo, O. M. 2004 A 'win-win' mechanism for low-drag transients in controlled two-dimensional channel flow and its implications for sustained drag reduction. *J. Fluid Mech.* **499**, 183–196.

Choi, H., Jeon, W.-P., & Kim, J. 2008 Control of flow over a bluff body. *Annu. Rev. Fluid Mech.* **40**, 113–139.

Choi, H., Moin, P. & Kim, J. 1994 Active turbulence control for drag reduction in wall bounded flows. *J. Fluid Mech.* **262**, 75–110.

Fukagata, K., Iwamoto, K. & Kasagi, N. 2002 Contribution of Reynolds stress distribution to the skin friction wall-bounded flows. *Phys. Fluids* **14**, L73–L76.

Fukagata, K. & Kasagi, N. 2002 Highly energy-conservative finite difference method for the cylindrical coordinate system. *J. Comput. Phys.* **181**, 478–498.

Fukagata, K. & Kasagi, N. 2003 Drag reduction in turbulent pipe flow with feedback control applied partially to wall. *Intl J. Heat Fluid Flow* **24**, 480–490.

Fukagata, K. & Kasagi, N. 2004 Suboptimal control for drag reduction via suppression of near-wall Reynolds shear stress. *Intl J. Heat Fluid Flow* **25**, 341–350.

Fukagata, K., Kasagi, N. & Koumoutsakos, P. 2006 A theoretical prediction of friction drag reduction in turbulent flow by superhydrophobic surfaces. *Phys. Fluids* **18**, 051703.

Fukagata, K., Sugiyama, K. & Kasagi, N. 2009 On the lower bound of net driving power in controlled duct flows. *Physica* D **238**, 1082–1086.

Gomez, T., Flutet, V. & Sagaut, P. 2009 Contribution of Reynolds stress distribution to the skin friction in compressible turbulent channel flows. *Phys. Rev.* E **79**, 035301.

Ham, F. E., Lien, F. S. & Strong, A. B. 2002 A fully conservative second-order finite difference scheme for incompressible flow on nonuniform grids. *J. Comput. Phys.* **177**, 117–133.

Hou, Y. X., Somandepalli, V. S. R. & Mungal, M. G. 2006 A technique to determine total shear stress and polymer stress profiles in drag reduced boundary layer flows. *Exp. Fluids* **40**, 589–600.

Hou, Y. X., Somandepalli, V. S. R. & Mungal, M. G. 2008 Streamwise development of turbulent boundary-layer drag reduction with polymer injection. *J. Fluid Mech.* **597**, 31–66.

Iwamoto, K., Suzuki, Y. & Kasagi, N. 2002 Reynolds number effect on wall turbulence: toward effective feedback control. *Intl J. Heat Fluid Flow* **23**, 678–689.

Kajishima, T. 2003 *Numerical Simulation of Turbulent Flows* (in Japanese), pp. 149–155. Yokendo.

Kasagi, N., Hasegawa, Y. & Fukagata, K. 2009 Toward cost-effective control of wall turbulence for skin friction drag reduction. *Advances in Turbulence XII*, Springer Proceedings in Physics, vol. 132, pp. 189–200. Springer.

Kasagi, N., Suzuki, Y. & Fukagata, K. 2009 Microelectromechanical systems-based feedback control of turbulence for skin friction reduction. *Annu. Rev. Fluid Mech.* **41**, 231–251.

Kim, J. 2003 Control of turbulent boundary layers. *Phys. Fluids* **15**, 1093–1105.

Kim, J. & Bewley, T. R. 2007 A linear systems approach to flow control. *Annu. Rev. Fluid Mech.* **39**, 383–417.

Kim, J. Kim, K. & Sung, H. J. 2003 Wall pressure fluctuations in a turbulent boundary layer after blowing or suction. *AIAA J.* **41**, 1697–1704.

Kim, J., Moin, P. & Moser, R 1987 Turbulence statistics in fully developed channel flow at low Reynolds number. *J. Fluid Mech.* **177**, 133–166.

Kim, K., Sung, H. J. & Chung, M. K. 2002 Assessment of local blowing and suction in a turbulent boundary layer. *AIAA J.* **40**, 175–177.

Kong, H., Choi, H. & Lee, J. S. 2000 Direct numerical simulation of turbulent thermal boundary layers. *Phys. Fluids* **12**, 2555–2568.

Lund, T. S., Wu, X. & Squires, K. D. 1998 Generation of turbulent inflow data for spatially developing boundary layer simulations. *J. Comput. Phys.* **140**, 233–258.

Lee, C., Kim, J. & Choi, H 1998 Suboptimal control of turbulent channel flow for drag reduction. *J. Fluid Mech.* **358**, 245–258.

Marusic, I., Mathis, R. & Hutchins, N. 2010 Predictive model for wall-bounded turbulent flow. *Science* **329**, 193–196.

https://doi.org/10.1017/jfm.2011.219 Published online by Cambridge University Press

Mehdi, F. & White, C. M. 2011 Integral form of the skin friction coefficient suitable for experimental data. *Exp. Fluids* **50**, 43–51.

Min, T., Kang, S. M., Speyer, J. L. & Kim, J. 2006 Sustained sub-laminar drag in a fully developed channel flow. *J. Fluid Mech.* **558**, 309–318.

Miyauchi, T., Tanahashi, M. & Suzuki, M. 1996 Inflow and outflow boundary conditions for direct numerical simulations. *JSME Intl J. Ser.* B **39**-2, 305–314.

Monty, J. P., Hutchins, N., Ng, H. C. H., Marusic, I. & Chong, M. S. 2009 A comparison of turbulent pipe, channel and boundary layer flow. *J. Fluid Mech.* **632**, 431–442.

Pamiès, M., Garnier, E., Merlen, A. & Sagaut, P. 2007 Response of a spatially developing turbulent boundary layer to active control strategies in the framework of opposition control. *Phys. Fluids* **19**, 108102.

Park, J. & Choi, H. 1999 Effects of uniform blowing or suction from a spanwise slot on a turbulent boundary layer flow. *Phys. Fluids* **11**, 3095–3105.

Peet, Y. & Sagaut, P. 2009 Theoretical prediction of turbulent skin friction on geometrically complex surfaces. *Phys. Fluids* **21**, 105105.

Quadrio, M. & Ricco, P. 2004 Critical assessment of turbulent drag reduction through spanwise wall oscillations. *J. Fluid Mech.* **521**, 251–271.

Schoenherr, K. E. 1932 Resistance of flat surfaces moving through a fluid. *Trans. Soc. Nav. Archit. Mar. Engrs* **40**, 279–313.

Spalart, P. R., Moser, R. D. & Rogers, M. M. 1991 Spectral methods for the Navier–Stokes equations with one infinite and two periodic directions. *J. Comput. Phys.* **96**, 297–324.

Stevenson, T. N. 1963 A law of the wall for turbulent boundary layers with suction and injection. *Aero. Rep.* 166. Cranfield College.

Sugiyama, K., Calzavarini, E. & Lohse, D. 2008 Microbubbly drag reduction in Taylor–Couette flow in the wavy vortex regime. *J. Fluid Mech.* **608** 21–41.

Sumitani, Y. & Kasagi, N. 1995. Direct numerical simulation of turbulent transport with uniform wall injection and suction. *AIAA J.* **33**, 1220–1228.

Wu, X. H. & Moin, P. 2009 Direct numerical simulation of turbulence in a nominally zero-pressure-gradient flat plate boundary layer. *J. Fluid Mech.* **630**, 5–41.

White, C. M. & Mungal, M. G. 2008 Mechanics and prediction of turbulent drag reduction with polymer additives. *Annu. Rev. Fluid Mech.* **40**, 235–256.

Xu, J., Dong, S., Maxey, M. & Karniadakis. G. E. 2007 Turbulent drag reduction by constant near-wall forcing. *J. Fluid Mech.* **582**, 79–101.

Yakeno, A., Hasegawa, Y. & Kasagi, N. 2009 In *Proceedings of the Sixth International Symposium on Turbulence and Shear Flow Phenomena*, Seoul.

Yu, B., Li, F. & Kawaguchi, Y. 2004 Numerical and experimental investigation of turbulent characteristics in a drag reducing flow with surfactant additives. *Intl J. Heat Fluid Flow* **25**, 961–974.

https://doi.org/10.1017/jfm.2011.219 Published online by Cambridge University Press